ISSN 1070-3284, Russian Journal of Coordination Chemistry, 2022, Vol. 48, No. 10, pp. 647–658. © Pleiades Publishing, Ltd., 2022.
Russian Text © The Author(s), 2022, published in Koordinatsionnaya Khimiya, 2022, Vol. 48, No. 10, pp. 632–644.

Dedicated to Academician Yu.A. Zolotov in the year of his 90th birthday

Synthesis, Crystal Structure, and Properties of Phenylsilicon(IV) Bis-catecholate Complexes

E. P. Kramarova[a], V. V. Negrebetskii[a], A. D. Volodin[b], P. A. Buikin[b, c], A. V. Lalov[d], R. A. Novikov[d], T. M. Aliev[b], A. A. Korlyukov[a, b], and A. V. Vologzhanina[b, *]

[a] *Pirogov Russian National Research Medical University, Moscow, Russia*
[b] *Nesmeyanov Institute of Organoelement Compounds, Russian Academy of Sciences, Moscow, Russia*
[c] *Kurnakov Institute of General and Inorganic Chemistry, Russian Academy of Sciences, Moscow, Russia*
[d] *Zelinsky Institute of Organic Chemistry, Russian Academy of Sciences, Moscow, Russia*
**e-mail: vologzhanina@mail.ru*

Received February 10, 2022; revised March 10, 2022; accepted March 15, 2022

Abstract—A series of anionic phenylsilicon(IV) bis-catecholate complexes, where $(Cat^1)^-$ = catecholate, $(Cat^2)^-$ = 3,4,5,6-tetrabromocatecholate, $(Cat^3)^-$ = 4-cyanocatecholate, $(Cat^4)^-$ = 4-nitrocatecholate, $(Cat^5)^-$ = 3-fluorocatecholate, and $(Cat^6)^-$ = 4,5-dibromocatecholate, were prepared by the reaction of trimethoxyphenylsilane with two equivalents of catechol or its derivatives containing electron-withdrawing substituents in the benzene ring in the presence of dicyclohexylamine. The complexes were characterized by IR spectra and ^1H, ^{13}C, and ^{29}Si NMR spectra, voltammetry, and ESR. The heteroligand anionic phenylsilicon(IV) complexes crystallized from solutions as salts $(Chex_2NH_2)[PhSi(Cat^1)_2]$ (**I**), $(Chex_2NH_2)[PhSi(Cat^2)_2]\cdot 0.5C_6H_{14}$ (**II**), $(Chex_2NH_2)[PhSi(Cat^3)_2]\cdot 2C_6H_6$ (**III**), $(Chex_2NH_2)[PhSi(Cat^4)_2]\cdot H_2O$ (**IV**), $(Chex_2NH_2)[PhSi(Cat^5)_2]$ (**V**), and $(Chex_2NH_2)[PhSi(Cat^6)_2]$ (**VI**) ($Chex_2NH_2^+$ = dicyclohexylammonium). The composition and structure of the products were confirmed by X-ray diffraction data (CCDC nos. 2150293–2150297 for **I**–**V**, respectively). The effect of substituent in the benzene ring on the electronic structure of the anion was studied by PBE0/6-311G(d,p) quantum chemical calculations with allowance for nonspecific solvation (PCM model). The oxidation potentials of **II**–**VI** were measured; radical formation upon electrochemical oxidation and reduction was observed for **II**.

Keywords: hypercoordinate silicon, catecholate anion, quantum chemical calculations, crystal structure

DOI: 10.1134/S1070328422090019

INTRODUCTION

Silicon complexes with catechol derivatives form an extensive class of compounds in which the silicon atom has coordination number of five or six. Most often, these complexes are anions and crystallize as salts with organic or alkali metal cations. Alkyl- and arylsilicon(IV) bis-catecholates have recently attracted research attention as sources of alkyl and aryl radicals in photocatalyzed cross-coupling reactions [1–8]. In most cases, alkylsilicon bis-catecholates were used as precursors, while the properties of arylsilicon bis-catecholates were studied only in [1, 8]. Data on substituent effects on the electrochemical and catalytic properties of compounds can be found only in [8]. We have shown that out of a number of substituted phenylsilicon bis-catecholates containing various electron-donating and electron-withdrawing moieties in the catecholate benzene ring, 4-cyanocatecholate complex was the best for elimination of the phenyl radical.

In this study, we obtained a series of dicyclohexylammonium salts of phenylsilicon bis-catecholates, studied their crystal structure and electrochemical properties, estimated the vertical and adiabatic ionization potentials by quantum chemical calculations, and considered the electronic structure of isolated anions and the corresponding oxidized species (neutral doublet radical semiquinone catecholate complexes).

EXPERIMENTAL

Commercial (Sigma Aldrich) catechol derivatives, dicyclohexylamine, C_6H_6, and C_6H_{14} (analytical grade) were used as received. IR spectra were measured using KBr on a Bruker Tensor-27 spectrometer. NMR spectra (^1H, 400 MHz; ^{13}C, 75 MHz) were recorded on a Bruker Avance II instrument in CD_3CN, DMSO-d_6, or $CDCl_3$ using Me_4Si as the

external standard. Melting points were determined on a Stuart SMP10 apparatus.

Dicyclohexylammonium salts were synthesized (Scheme 1) by the reaction of trimethoxyphenylsilane with catechol (Cat^1) and its derivatives (Cat^n; n = 2–6 for 3,4,5,6-tetrabromocatechol, 4-cyanocatechol, 4-nitrocatechol, 3-fluorocatechol, and 4,5-dibromocatechol, respectively) in the presence of dicyclohexylamine at the boiling temperature of the solvent (xylene or acetonitrile).

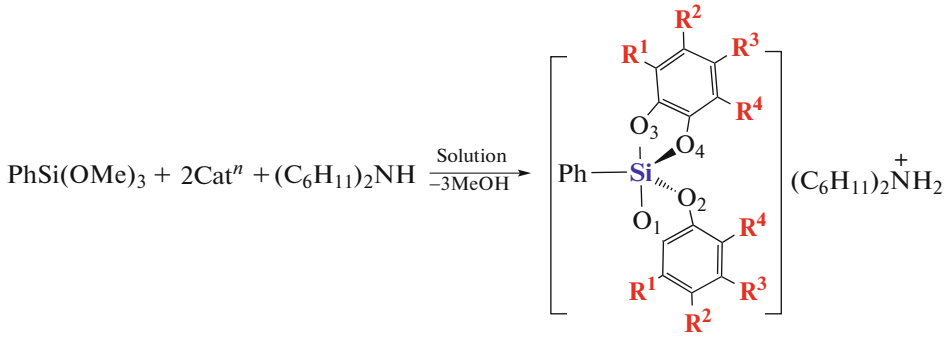

I: $R^1 = R^2 = R^3 = R^4 = H$
II: $R^1 = R^2 = R^3 = R^4 = Br$
III: $R^1 = R^2 = R^4 = H$; $R^3 = CN$
IV: $R^1 = R^2 = R^4 = H$; $R^3 = NO_2$
V: $R^2 = R^3 = R^4 = H$; $R^1 = F$
VI: $R^1 = R^4 = H$; $R^2 = R^3 = Br$

Scheme 1.

Synthesis of dicyclohexylammonium bis(phenyl-1,2-diolato-O,O')phenylsilicate(IV), $(Chex_2NH_2)[PhSi(Cat^1)_2]$ (I). A mixture of trimethoxyphenylsilane (3.96 g, 0.02 mol), catechol (4.4 g, 0.04 mol), and dicyclohexylamine (3.62 g, 0.02 mol) in xylene (10 mL) was refluxed for 30 min. The next day the reaction mixture was poured into hexane (70 mL). The precipitated crystals were collected on a filter. The yield of **I** was 6.2 g (62%). T_m = 272–275°C. The crystals suitable for X-ray diffraction were grown from CH_3CN.

IR (ν, cm^{-1}): 1599 w (Ph), 1483 s, 1460 w (NH_2^+), 1236 s (PhO). ^1H NMR (DMSO-d_6; δ, ppm): 1.0–1.5 (m, 12H), 1.50–2.00 (m, 8H), 2.00 (m, 2H), 6.50–7.54 (m, 12H). ^{13}C NMR (DMSO-d_6; δ, ppm): 24.55, 25.53, 30.54, 52.61, 109.14, 110.26, 115.47, 116.12, 117.96, 119.71, 127.23, 128.28, 133.82, 135.23, 142.28, 145.76, 150.85. ^{29}Si NMR (DMSO-d_6; δ, ppm): –87.55.

Synthesis of dicyclohexylammonium bis(3,4,5,6-tetrabromophenyl-1,2-diolato-O,O')phenylsilicate(IV) *n*-hexane hemi-solvate, $(Chex_2NH_2)[PhSi(Cat^2)_2]\cdot 0.5C_6H_{14}$ (II). A mixture of trimethoxyphenylsilane (0.198 g, 0.001 mol), 3,4,5,6-tetrabromocatechol (0.83 g, 0.002 mol), and dicyclohexylamine (0.18 g, 0.001 mol) in acetonitrile (5 mL) was refluxed for 2 h. After 24 h, the mixture was evaporated on a rotary evaporator. The residue was triturated with hexane until crystals formed. The yield of **II** was 0.59 g (52%). T_m = 228–230°C. The crystals suitable for X-ray diffraction were grown from dioxane.

IR (ν, cm^{-1}): 1556 w (Ar), 1447 s (NH_2^+) 1272 w, 1223 w (ArO). ^1H NMR (CD_3CN; δ, ppm): 1.10–1.24 (m, 2H), 1.31 (m, 8H), 1.66 (dm, J = 12.4 Hz, 2H), 1.74–1.88 (m, 4H), 1.94–2.07 (m, 4H), 3.19 (s, 2H), 6.38 (t, J = 37.6 Hz, 2H), 7.32–7.34 (m, 3H), 7.52–7.59 (m, 2H). ^{13}C NMR (CD_3CN; δ, ppm): 24.95, 25.57, 30.04, 55.25, 107.26, 115.73, 128.72, 130.41, 135.54, 138.30, 149.43. ^{29}Si NMR (CD_3CN; δ, ppm): –85.8.

HRMS (m/z) calcd.: 952.3349, for $C_{18}H_5O_4SiBr_8$, found: 952.3316.

Synthesis of dicyclohexylammonium bis(4-cyanophenyl-1,2-diolato-O,O')phenylsilicate(IV) benzene disolvate, $(Chex_2NH_2)[PhSi(Cat^3)_2]\cdot 2C_6H_6$ (III). A mixture of 4-cyanocatechol (1.35 g, 0.01 mol), dicyclohexylamine (0.9 g, 0.005 mol), and trimethoxyphenylsilane (0.99 g, 0.005 mol) in acetonitrile (15 mL) was refluxed for 2 h. After 24 h, the mixture was concentrated on a rotary evaporator. The residue was triturated with petroleum ether. The yield of **III** was 2.45 g (89%). T_m = 252–254°C. The crystals suitable

for X-ray diffraction were grown from a 6 : 1 C_6H_6–CN mixture.

IR (ν, cm^{-1}): 2214 s (CN), 1601 m (Ar), 1487 s $\left(NH_2^+\right)$, 1260 s (ArO). ^1H NMR (CD_3CN; δ, ppm): 1.05–1.42 (m, 10H), 1.65 (d, J = 11.7 Hz, 2H), 1.73.–1.87 (m, 4H), 2.00. 2.12 (m, 4H), 3.16–3.31 (m, 2H), 6.82–6.91 (m, 2H), 7.03–7.14 (m, 4H), 7.19–7.31 (m, 3H), 7.51–7.58 (m, 2H). ^{13}C NMR (CD_3CN; δ, ppm): 25.01, 25.61, 30.13, 55.15, 100.91, 101.33, 111.91, 112.02, 113.77, 113.91, 121.42, 125.94, 126.31, 128.36, 129.83, 135.29, 140.35, 151.01, 151.36, 156.00, 156.38. ^{29}Si NMR (CD_3CN; δ, ppm): –85.23.

HRMS (*m/z*) calcd.: 371.0494, for $C_{20}H_{11}N_2O_4Si$ found: 371.0486.

Synthesis of dicyclohexylammonium bis(4-nitrophenyl-1,2-diolato-O,O')phenylsilicate(IV) monohydrate, $(Chex_2NH_2)[PhSi(Cat^4)_2]\cdot H_2O$ (IV). A mixture of trimethoxyphenylsilane (0.5 g, 0.0025 mol), 4-nitrocatechol (0.77 g, 0.005 mol), and dicyclohexylamine (0.45 g, 0.0025 mol) in xylene (10 mL) was refluxed for 40 min. After 24 h, the mixture was concentrated. The resulting thick oil was crystallized by trituration in petroleum ether. The yield of **IV** was 1 g (67%). T_m = 12–215°C (dec.). The crystals suitable for X-ray diffraction were grown by evaporation of an CH_3CN solution.

IR (ν, cm^{-1}): 1592 m (Ar), 1485 s $\left(NH_2^+\right)$ 1265 s (ArO). ^1H NMR (CD_3CN; δ, ppm): 1.06–1.45 (m, 10H), 1.64 (d, J = 12.4 Hz, 2H), 1.73–1.85 (m, 4H), 1.99–2.10 (m, 4H), 3.15–3.30 (m, 2H), 6.86 (dd, J = 8.6, 4.4 Hz, 2H), 7.17–7.31 (m, 3H), 7.58 (dd, J = 7.4, 2.1 Hz, 2H), 7.64 (dd, J = 4.8, 2.6 Hz, 2H), 7.76 (td, J = 8.9, 2.7 Hz, 2H). ^{13}C NMR (CD_3CN; δ, ppm): 25.02, 25.61, 30.04, 55.20, 105.39, 106.38, 106.67, 109.68, 110.26, 110.44, 117.43, 117.93, 118.58, 128.44, 129.31, 129.99, 135.35, 139.89, 140.47, 140.96, 150.37, 150.94, 158.36, 158.98. ^{29}Si NMR (CD_3CN; δ, ppm): –83.52.

HRMS (*m/z*) calcd.: 411.0290, for $C_{18}H_{11}N_2O_8Si$ found: 411.0286.

Synthesis of dicyclohexylammonium bis(3-fluorophenyl-1,2-diolato-O,O')phenylsilicate(IV) monohydrate $(Chex_2NH_2)[PhSiCat^5_2]$ (V). A mixture of trimethoxyphenylsilane (1 g, 0.005 mol), 3-fluorocatechol (1.28 g, 0.01 mol), and dicyclohexylamine (0.9 g, 0.005 mol) in acetonitrile (10 mL) was refluxed for 2 h. After 24 h, the crystalline product was collected on a filter. The yield of **V** was 2.13 g (79%). T_m = 238–241°C. The crystals suitable for X-ray diffraction were grown from CH_3CN.

IR (ν, cm^{-1}): 1625 m, 1601 w (Ar), 1494 s, 1472 s $\left(NH_2^+\right)$, 1268 s ArO. ^1H NMR (DMSO-d_6; δ, ppm): 1.18 (m, 10H), 1.59 (d, J = 12.6 Hz, 2H), 1.71 (d, J = 12.1 Hz, 4H), 1.91 (d, J = 10.8 Hz, 4H), 2.85–3.00 (m, 2H), 6.35–6.66 (m, 6H), 7.12–7.25 (m, 3H), 7.44–7.59 (m, 2H). ^{13}C NMR (DMSO-d_6; δ, ppm): 24.14, 25.12, 30.24, 52.28, 105.91 (dd, J = 18.0, 11.2 Hz), 106.41 (d, J = 14.2 Hz), 106.55 (d., J = 2.8 Hz), 111.45 (d, J = 2.4 Hz), 116.72 (dd, J = 13.2, 8.1 Hz), 118.16 (d, J = 9.5 Hz), 127.07, 128.31, 133.57 (d, J = 13.8 Hz), 134.67, 136.81, 140.43, 146.41, 147.95 (d, J = 5.6 Hz), 149.58, 150.71, 152.60 (dd, J = 9.2, 7.2 Hz), 153.85.

^{29}Si NMR (DMSO-d_6; δ, ppm): –84.94.

HRMS (*m/z*) calcd.: 357.0400, for $C_{18}H_{11}F_2O_4Si$ found: 357.0396.

Synthesis of dicyclohexylammonium bis(4,5-dibromophenyl-1,2-diolato-O,O')phenylsilicate(IV), $(Chex_2NH_2)[PhSi(Cat^6)_2]$ (VI). A mixture of trimethoxyphenylsilane (0.5 g, 0.0025 mol), 4,5-dibromocatechol (1.38 g, 0.005 mol), and dicyclohexylamine (0.45 g, 0.0025 mol) in acetonitrile (10 mL) was refluxed for 2 h. After 24 h, the reaction mixture was concentrated. The residue was crystallized by trituration in petroleum ether. The yield of **VI** was 1.86 g (92%). T_m = 205–207°C (reprecipitation of a dioxane solution of compound **VI** in petroleum ether).

IR (ν, cm^{-1}): 1595 s (Ar), 1477 s, 1448 m $\left(NH_2^+\right)$, 1231 (ArO). ^1H NMR (CD_3CN; δ, ppm): 1.05–1.46 (m, 10H), 1.59–1.70 (m, 2H), 1.71–1.91 (m, 4H), 2.04 (d, J = 8.2 Hz, 4H), 3.12–3.31 (m, 2H), 7.06 (s, 3H), 7.18–7.29 (m, 3H), 7.46–7.56 (m, 2H).

^{13}C NMR (CD_3CN, δ, ppm): 25.00, 25.59, 29.99, 55.07, 111.77, 115.58, 128.30, 135.15, 140.38, 146.37, 151.88. ^{29}Si NMR (CD_3CN; δ, ppm): –84.53.

HRMS (*m/z*) calcd.: 636.6970, for $C_{30}H_{33}Br_4NO_4Si$, found: 636.6960.

X-ray diffraction study was carried out on a Bruker APEX DUO diffractometer (graphite monochromator, $\lambda(CuK_\alpha)$ = 1.54178 Å (**I**), $\lambda(MoK_\alpha)$ = 0.71073 Å (**III**)) at 120.0(2) K and a Bruker D8 QUEST diffractometer (graphite monochromator, $\lambda(MoK_\alpha)$ = 0.71073 Å (**II**, **IV**, **V**) at 100.0(2) K. Semiempirical absorption corrections were applied by the R. Blessing procedure [9] using SADABS software [10]. Structure solution and refinement were performed using ShelX-2014 OLEX2 software packages [11]. The structures were solved by the intrinsic phasing method (ShelXT program [12]) and refined by least-squares method (ShelXL program [13]). The positions and thermal parameters of non-hydrogen atoms were refined in the isotropic and then anisotropic approximation by the full-matrix least squares method. Fluorine atoms in the two independent anions of 3-fluorocatecholate were disordered over two positions with 0.384 : 0.616 occupancy ratio (refined as independent variable). All hydrogen atoms were calculated according to their idealized geometry and refined with constraints applied on the CH bond lengths and isotropic dis-

Table 1. Crystallographic data and X-ray experiment and structure refinement details for **I**–**V**

Parameter	Value				
	I	**II**	**III**	**IV**	**V**
Molecular formula	$C_{30}H_{37}NO_4Si$	$C_{33}H_{36}NO_4SiBr_8$	$C_{44}H_{47}N_3O_4Si$	$C_{30}H_{37}N_3O_9Si$	$C_{30}H_{35}F_2NO_4S$
M	503.69	1178.00	709.93	611.71	539.68
Space group	$I4_1/a$	$P\bar{1}$	$P2_1/c$	$P2_1/c$	$Pbca$
a, Å	19.4077(4)	12.5736(14)	10.5358(7)	14.7233(3)	10.6333(3)
b Å	19.4077(4)	13.6301(16)	20.3097(17)	11.4826(3)	16.0600(5)
c Å	28.3974(9)	13.877(2)	18.3939(14)	17.6464(5)	32.0397(10)
α, deg	90	60.703(4)	90	90	90
β, deg	90	67.288(6)	102.318(2)	99.6410(10)	90
γ, deg	90	77.553(4)	90	90	90
V, Å^3	10696.1(6)	1912.2(5)	3845.3(5)	2941.20(13)	5471.4(3)
ρ(calcd.), g/cm^3	1.251	2.046	1.226	1.381	1.310
μ, mm^{-1}	1.059	8.457	0.108	0.140	0.136
Scanning range of θ, deg	5.516–30.238	3.428–52.044	3.026–55.082	4.524–55.756	4.766–61.042
Number of collected reflections	14258	7487	16836	26510	34239
Number of unique reflections	4163	7487	16836	7000	8363
R_{int}	0.0716			0.0426	0.0956
GOOF	1.012	1.036	1.056	1.055	1.040
R_1 ($I > 2\sigma(I)$)	0.0439	0.0706	0.0890	0.0670	0.0579
wR_2 (for all data)	0.1152	0.1921	0.1992	0.1838	0.1335
Residual electron density (min/max), e Å^{-3}	0.20/–0.27	1.35/–1.25	0.38/–0.38	0.83/–0.44	0.36/–0.42

placement parameters (U_{iso} (H) = 1.2U_{equiv} (C) for CH_2 and CH; U_{iso} (H) = 1.5U_{equiv} (C) for CH_3). Crystallographic data and main refinement parameters for compounds **I**–**V** are summarized in Table 1.

Additional crystallographic data for structures **I**–**V** are deposited with the Cambridge Crystallographic Data Centre (CCDC nos. 2150293–2150297; http://www.ccdc.cam.ac.uk/structures).

Electrochemical measurements were carried out using an Autolab PGSTAT128N potentiostat galvanostat with the NOVA 2.0 software package and a conventional three-electrode cell. A glassy carbon working electrode, an Ag/AgCl reference electrode (in a saturated KCl solution), and a platinum wire as the counter electrode were used. A 0.1 M solution of $TBAPF_6$ in DMSO served as the supporting electrolyte. All measurements were carried out at a potential sweep rate of 100 mV/s. Prior to each experiment, the test solution was purged with nitrogen gas for 5 min and the working electrode was thoroughly polished. All measurements were carried out at room temperature. The measured potentials were referred to the Fc/Fc^+ pair.

ESR spectra were recorded on a Bruker EMX 6/1 instrument equipped with a standard ER4102ST rectangular cavity with the central frequency of 9.8 GHz.

Quantum chemical studies. The geometries of anions **I**–**VI** and their oxidized forms in the doublet state were optimized by the PBE0 hybrid functional and the 6-311G(d,p) basis set using the Q-Chem 5.4 program [14, 15]. The extension of the basis set by additional diffuse functions led to a considerable increase in the computational cost and to convergence problems caused by the linear dependence, especially in the case of brominated anions; however, no significant difference in the optimized geometry was observed in comparison with the 6-311G(d,p) basis set optimization. The general protocol of quantum chemical calculations, described in detail in [16], included geometry optimization with allowance for the solvent effect (PCM/DMSO), calculation of harmonic frequencies, and thermochemical analysis as described in

[16]. The optimization was done using the empirical dispersion correction D3. The total energies of anions and their oxidized forms obtained in this way were used to calculate the first oxidation potentials. The electron-withdrawing effect was considered by analyzing the mean local ionization energy, which was calculated using the Multiwfn program [17]; drawings were made by the VMD program [18].

RESULTS AND DISCUSSION

The reactions of catechol (2 mol) or its commercially available derivatives with various electron-withdrawing substituents in the benzene ring with trimethoxyphenylsilane(IV) (1 mol) in the presence of dicyclohexylamine (1 mol) take place on refluxing in acetonitrile or xylene and form salts $(Chex_2NH_2)$-$[PhSi^{IV}(Cat^x)_2]^-$ (**I**–**VI**, $Chex_2NH_2^+$ = bis-cyclohexylammonium, x = 1–6, Scheme 1). The yield of the target products varies from 52 to 89%, which is in good agreement with the data reported previously for bis-catecholate phenylsilicates(IV) [8]. The composition of the obtained complexes was confirmed by ^1H, ^{13}C, and ^{29}Si NMR spectroscopy and by high-resolution mass spectrometry data. According to the ^{29}Si NMR data, the silicon signal is shifted downfield to the –82 to –88 ppm range, characteristic of five-coordinate silicon atoms.

The X-ray diffraction data for compounds **I**–**V** prepared as single crystals confirm that the $[PhSi^{IV}(Cat^x)_2]^-$ complex anions contain a five-coordinate silicon(IV) atom bound to the phenyl group and two catecholate anions. As a result, the cations and anions in structures **I**–**V** occur in 1 : 1 ratio; in addition, the crystals of **II**–**IV** contain hexane, benzene, or water solvate molecules, respectively. In all cases, the structural units occupy general positions. The independent part of the unit cells is shown in Fig. 1.

Like in the phenylsilicon(IV) bis-catecholate complexes structurally characterized previously [1, 8, 19–21], in these complexes, the catecholate anions act as bidentate chelating ligands, being bound to the central atom by two oxygen atoms, while the phenyl group is a terminal ligand. Thus, the silicon(IV) atom forms the $Si^{IV}CO_4$ coordination polyhedron the vertices of which are occupied by the oxygen atoms of two different catecholate anions (Fig. 1). The shape of the spirocyclic coordination polyhedron of five-coordinate silicon is identified, most often, by calculating the Berry coordinate, in which a particular coordination polyhedron is represented as a point in the transition coordinate between square pyramid (SP) and trigonal bipyramid (TBP) [22]. The value of the Berry coordinate, which can be estimated through the solid angle of faces of the coordination polyhedron, shows the contribution of TBP in %. The calculated Berry coordinates for **I**–**V** were 84.5, 92.0, 84.5, 49.6, and 76.9%; that is, only for compound **IV**, the $Si^{IV}CO_4$ polyhedron is intermediate between TBP and SP, and for complex **V**, SP makes a significant contribution to the coordination polyhedron shape. Meanwhile in other compounds, the coordination geometry can be considered to be distorted TBP. The Si–O bond lengths generally vary from 1.70(1) to 1.820(5) Å and are shorter than the Si–C bonds (Fig. 2). The oxygen atoms characterized by OSiO bond angles closer to 180° were chosen as axial vertices, because only in **IV**, **V**, and $(Me_4N)[PhSi^{IV}(Cat^1)_2]$ [19], the bonds could be subdivided into longer axial and shorter equatorial ones on the basis of the bond lengths. In other complexes, the equatorial and axial bond lengths may coincide within 3σ. The $O_{ax}SiO_{ax}$ angle varies from 149.3(1)° (**III**) to 167.7(1)° ($(Me_4N)[PhSi^{IV}(Cat^1)_2]$), with the deviation from linearity being due to repulsion from the phenyl group. The $CSiO_{ax}$ angle is not smaller than 99.1(1)°, while the $CSiO_{eq}$ angle is 105.0(1)°–115.3(1)°. Comparison of the lengths of equivalent coordination bonds shows that the geometry of the coordination unit of silicon largely depends on the nature of the substituents in the benzene ring of the catecholate ligand and the presence of strong hydrogen bonds, while the Si–C coordination bond remains invariable within 3σ. This is in line with published data, indicating that the geometry of hypercoordinate silicon complexes is strongly affected by intermolecular interactions in the crystal or in solution [23]. Even in the case of unsubstituted catecholate ligand in the absence of strong hydrogen bonds, the lengths of the axial and equatorial bonds can coincide as in the complex $K[PhSi^{IV}(Cat^1)_2]\cdot 2Me_2CO$ [1], or can be sharply different as in $(Me_4N)[PhSi^{IV}(Cat^1)_2]$ [19]. In the same way, the equatorial and axial bond lengths in $(Et_4N)[PhSi^{IV}(Cat^7)_2]$ (Cat^7 = 3,4,5,6-tetrachlorocatecholate) [21], in which there are no strong hydrogen bonds, are similar. A pronounced variation of the Si–O coordination bond length is observed in complexes with electron-donating substituents in the benzene ring of structures **IV** (Cat^4 = 4-nitrocatecholate) and $(Et_3NH)[PhSi^{IV}(Cat^8)_2]$ (Cat^8 = 3,5-di-*tert*-butylcatecholate) [20]. In compound **III**, along with strong hydrogen bonds, one can assume the presence of strong agostic C–H...Si contacts involving the benzene solvate molecule, because in both disordered moieties, a hydrogen atom of the solvate molecule is located in the continuation of the C_{Ph}–Si bond (the C_{Ph}–Si...H angle is 158.0°–167.6°, r(Si...C) is 3.871(7)–3.899(12) Å) and completes the 5 + 1 coordination of the central atom (Fig. 3). As a result, the Si coordination polyhedron in this compound is rather a square pyramid and the Si–O bond lengths are approximately equal.

Visualization of the coordination unit distortions and comparison of the conformations of the anionic complex as a whole is shown in Fig. 4, in which the sil-

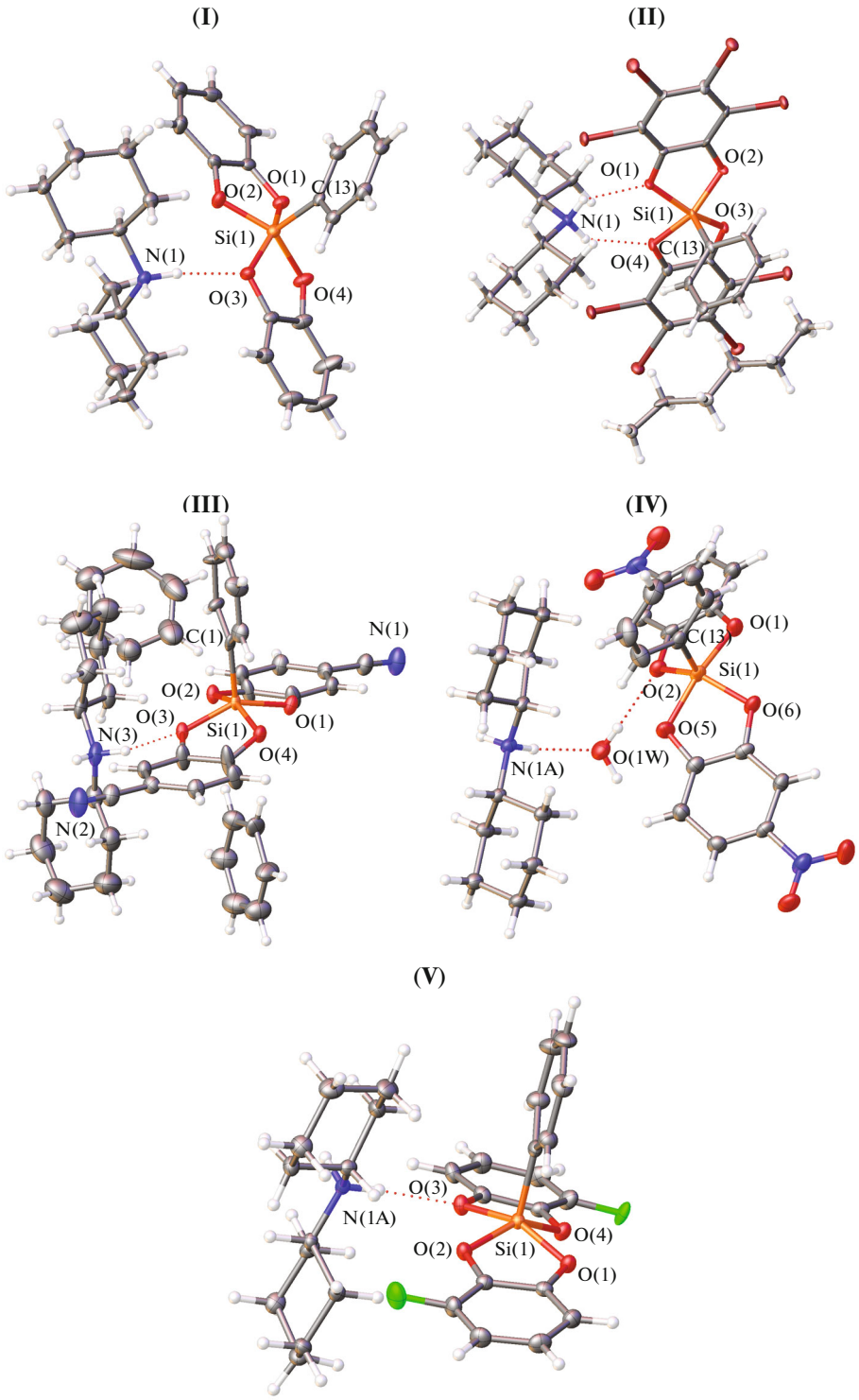

Fig. 1. Independent part of cells in structures **I**–**V** with atoms represented by thermal ellipsoids (p = 50%). For compounds **III** and **V**, one of the two disordered parts of the anion and benzene solvate molecule is shown.

icon(IV) coordination polyhedra are superimposed onto one another. The position of the phenyl group reflects the facts that it can freely rotate relative to the Si–C single bond and that the C_{Ph}–H...O_{Cat} bond energy is either absent or low. Meanwhile, despite the rigid planar conformation of particular catecholate anions, their relative positions at the silicon atom also markedly vary depending on the substituents in the

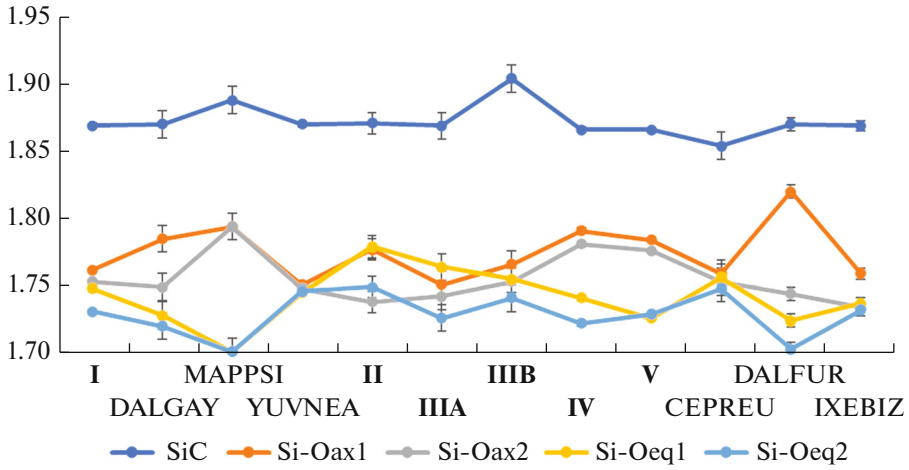

Fig. 2. Lengths of Si–C and Si–O coordination bonds with axial and equatorial oxygen atoms in structures **I**–**V** and in previously described complexes $(Me_4N)[PhSi^{IV}(Cat^1)_2]$ {MAPPSI} [19], $K[PhSi^{IV}(Cat^1)_2]\cdot 2Me_2CO$ {YUVNEA} [1], $(Et_3NH)[PhSi^{IV}(Cat^1)_2]$ {DALGAY} [20], $(Et_3NH)[PhSi^{IV}(Cat^8)_2]$ {DALFUR} [20], $(Et_4N)[PhSi^{IV}(Cat^7)_2]$ {CEPREU} [21], and (Kcrow)(Kcrow(Me_2CO))$[PhSi^{IV}(Cat^5)_2]_2$ {IXEBIZ} [8]. Cat^6 = 3,4,5,6-tetrachlorocatecholate, Cat^7 = 3,5-di-*tert*-butylcatecholate, crow = 18-crown-6. The letters stand for the codes of the compound in CCDC. The experimental error of bond determination is marked.

benzene ring and the crystal environment. The conformations of $[PhSi^{IV}(Cat^R)_2]^-$ in **I**, $(Me_4N)[PhSi^{IV}(Cat^1)_2]$ [19], $K[PhSi^{IV}(Cat^1)_2]\cdot 2Me_2CO$ [1], and $(Et_3NH)[PhSi^{IV}(Cat^1)_2]$ [20] also differ from one another (see Fig. 4).

The influence of specific interactions can be traced by comparing equivalent bonds that either participate or not participate in strong contacts. Indeed, in the crystals of previously synthesized and structurally characterized acetamide- and caprolactam-containing silicon catecholates [24, 25], the Si–O bonds to catecholate anions involved in classical type hydrogen bonds (O–H···O and N–H···O) are, as a rule, 0.1 Å longer than the bonds not involved in contacts of this type. In complexes **I**–**V**, the presence of hydrogen donor atoms in the cation and some acceptor atoms in the anions results in the formation of hydrogen bonds in all compounds; the parameters of these bonds are

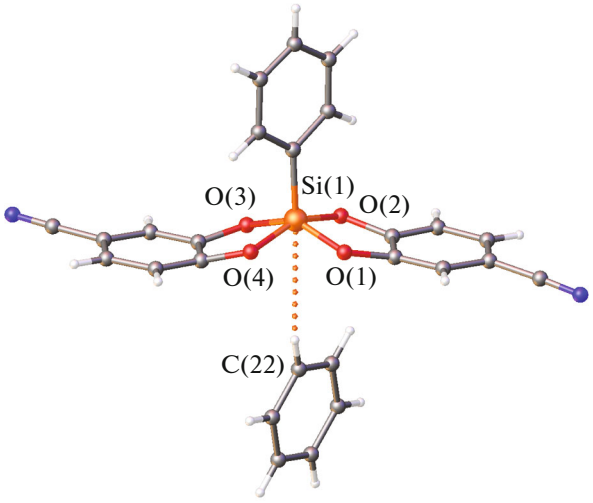

Fig. 3. Agostic interactions in structure **III**. The Si...H contact is shown by dashed line. One position of the two disordered positions is shown.

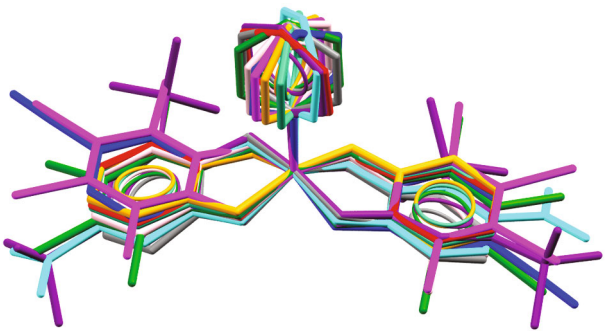

Fig. 4. Conformations of the $[PhSi^{IV}(Cat^R)_2]^-$ anions in structures **I** (red), **II** (fuchsia), **III** (blue), **IV** (light blue), **V** (lilac), $(Me_4N)[PhSi^{IV}(Cat^1)_2]$ (gray) [19], $K[PhSi^{IV}(Cat^1)_2]\cdot 2Me_2CO$ (emerald) [1], $(Et_3NH)[PhSi^{IV}Cat^1_2]$ (orange) [20], $(Et_3NH)[PhSi^{IV}Cat^5_2]$ (violet) [20], $(Et_4N)[PhSi^{IV}Cat^6_2]$ (green) [21], (Kcrow)(Kcrow(Me_2CO))$[PhSi^{IV}Cat^7_2]_2$ (pink) [8]. Hydrogen atoms are not shown. The atoms of the $Si^{IV}CO_4$ coordination polyhedron are superimposed on one another.

Table 2. Geometric parameters of hydrogen bonds in structures **I**–**V***

D–H...A	Distance, Å			DHA angle, deg
	D–H	H...A	D...A	
		I		
N(1)–H(1A)...O(3)	0.94	1.96	2.885(2)	169
N(1)–H(1B)...O(1)^{i}	0.94	2.20	3.024(2)	154
N(1)–H(1B)...O(4)^{i}	0.94	2.30	3.070(3)	144
		II		
N(1)–H(1A)...O(1)^{ii}	0.91	2.19	2.930(11)	138
N(1)–H(1B)...O(4)^{ii}	0.91	2.18	2.924(14)	138
		III		
N(3)–H(3B)...O(3)	0.91	2.14	3.012(10)	160
N(3)–H(3B)...O(3A)	0.91	1.98	3.012(10)	168
N(3)–H(3C)...N(1)^{iii}	0.91	2.13	3.027(4)	170
		IV		
O(1W)–H(1WA)...O(2)	0.85	2.07	2.912(3)	171
O(1W)–H(1WB)...O(7)^{iv}	0.91	2.15	2.964(3)	157
N(1)–H(1AB)...O(1W)	0.91	1.98	2.804(3)	157
N(1)–H(1AA)...O(3)^{v}			3.013(3)	159
		V		
N(1A)–H(1B)...O(3)			2.870(2)	166
N(1A)–H(1A)...O(1)^{vi}	0.91	2.00	2.903(2)	175

* Symmetry codes: ^{i} $5/4 - y, -1/4 + x, -1/4 + z$; ^{ii} $1 - x, 1 - y, 1 - z$; ^{iii} $-1 + x, 3/2 - y, -1/2 + z$; ^{iv} $2 - x, 1 - y, 1 - z$; ^{v} $x, 5/2 - y, -1/2 + z$; ^{vi} $1/2 - x, 1/2 + y, z$.

given in Table 2. The cation in **II** forms two hydrogen bonds with the oxygen atoms of two different catecholate anions within one complex ion, thus giving a hydrogen-bonded island group (Fig. 5). Complexes **I**, **III**, and **V** have hydrogen-bonded infinite chins in their structure (Fig. 6). In **I**, one proton is bound to the O(3) atom of one anion, while the second proton forms a bifurcated bond with the O(1) and O(4) atoms of another anion. In **III**, the cation forms two hydrogen bonds and occupies a bridging position between the O(3) (or O(3A)) atom of one anion and the cyano-group N(1) atom of the other anion. In **V**, the H(N) atoms interact with the oxygen atoms of the axial Si–O_{ax} bonds. Owing to the presence of water molecule in **IV**, a layered hydrogen-bonded moiety is formed, although the cation participates only in two hydrogen bonds (Fig. 5). The water molecule participates in three hydrogen bonds as a donor of two protons and a hydrogen bond acceptor. The complex anion in **IV** is an acceptor of three hydrogen bonds involving one catecholate anion and oxygen atoms of two nitro groups. In hydrogen-bonded layers (Fig. 5), it is possible to distinguish four-membered rings comprising two water molecules and two anions and twelve-membered rings comprising four water molecules, four cations, and four anions. If the network is simplified to 3,3-coordinated one (by simplifying the bridging cations), its topology can be classified as **fes**, according to the Reticular Chemistry Structure Resource system [26]. The participation of the catecholate oxygen atom in hydrogen bonding induces elongation of the Si–O bond with the hydrogen bond acceptor oxygen. As can be seen in Fig. 2, the difference between the lengths of axial and equatorial bonds is 0.02 to 0.08 Å (on average, 0.03 Å), whereas the difference between the lengths of coordination bonds with oxygen atoms not involved (or both involved) in hydrogen bonds is, on average, 0.01 Å.

A relevant application of five-coordinate silicon complexes is to initiate polymerization reactions by generation of radical species. The tendency for this behavior should be determined by the nature of substituents at the silicon atom, which can influence stabilization of oxidized **I**–**VI** in different ways. Compounds **II**–**VI** contain different numbers of electron-withdrawing groups, which can have not only inductive, but also mesomeric effect. In order to study the effect of substituents on the electronic structure, quantum chemical calculations were carried out for

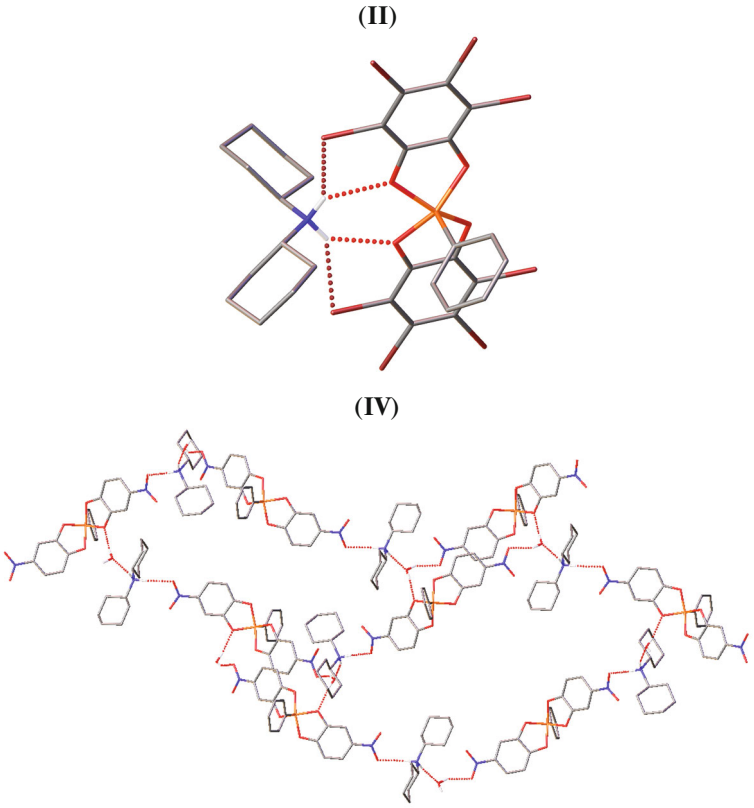

Fig. 5. Hydrogen-bonded architectures in structures **II** and **IV**. The hydrogen atoms not involved in hydrogen bonds are omitted.

the unoxidized free anions **I**–**VI** and their oxidized forms **I***–**VI***.

Geometry optimization of the anions and their oxidized forms carried out using the PBE0/6-311G(d,p) method demonstrated that the lengths of axial Si–O bonds differ from equatorial bond lengths by 0.03–0.06 Å, while the coordination polyhedron retains the trigonal bipyramidal shape. Generally, the difference between the axial and equatorial Si–O bond lengths somewhat increases with increasing number of electron-withdrawing substituents. Nevertheless, the influence of substituents on the silicon coordination geometry is relatively slight (Tables S1–S6). In the oxidized forms, the difference between the axial and equatorial bond lengths increases, being also dependent on the ligand. The Si–O(1) and Si–O(2) bond lengths in **I***–**VI*** differ from each other to a much greater extent than the Si–O(3) and Si–O(4) bond lengths. Upon the removal of an electron, the axial Si–O(1) bond proved to be 0.02–0.03 Å shorter than the equatorial Si–O(2) bond. Conversely, the axial Si–O(3) bond is 0.11–0.12 Å longer than the equatorial bond. The oxidation also leads to shortening of the Si–C bond (by 0.02–0.03 Å).

Analysis of the frontier orbitals of anionic complexes **I**–**VI** showed that vertical ionization mainly affects the region of catecholate ligands. Indeed, the greatest HOMO and LUMO occupancies are observed for the carbon atoms of the phenyl substituents and the catecholate oxygen atoms (Fig. 7). In **I***–**VI***, the spin density maxima (Fig. 8) are located on the oxygen and carbon (position 3) atoms of the catecholate ligand.

The Si–O bond length distribution in **I***–**VI*** indicates that the electron-withdrawing properties of one of the catecholate ligands is markedly reduced. The ability of this ligand to interact with electrophilic agents and free radicals also decreases. To illustrate this ability, P. Politzer proposed the value of average local ionization energy (ALIE) [27]. Figure 9 shows the superimposition of the distribution of the ALIE function on the electron density isosurface (ρ = 0.005 a.u.) for anion **III** and its oxidized form. The ALIE minima correspond to the preferred positions of the electrophilic attack. The ALIE minima in **III** are located around the phenyl group and around the carbon atoms (positions 2 and 5) of the catecholate ligands. In the case of **III***, the decrease in the size of ALIE minimum compared to **III** reflects decrease in the reactivity towards electrophiles and free radicals.

The oxidation potential is determined by the vertical and adiabatic ionization potentials, which, according to quantum chemical calculations, explicitly depend on the nature of the substituent. The highest vertical ionization potential is found for **VI** with the dibromocatecholate ligand, while the lowest value is

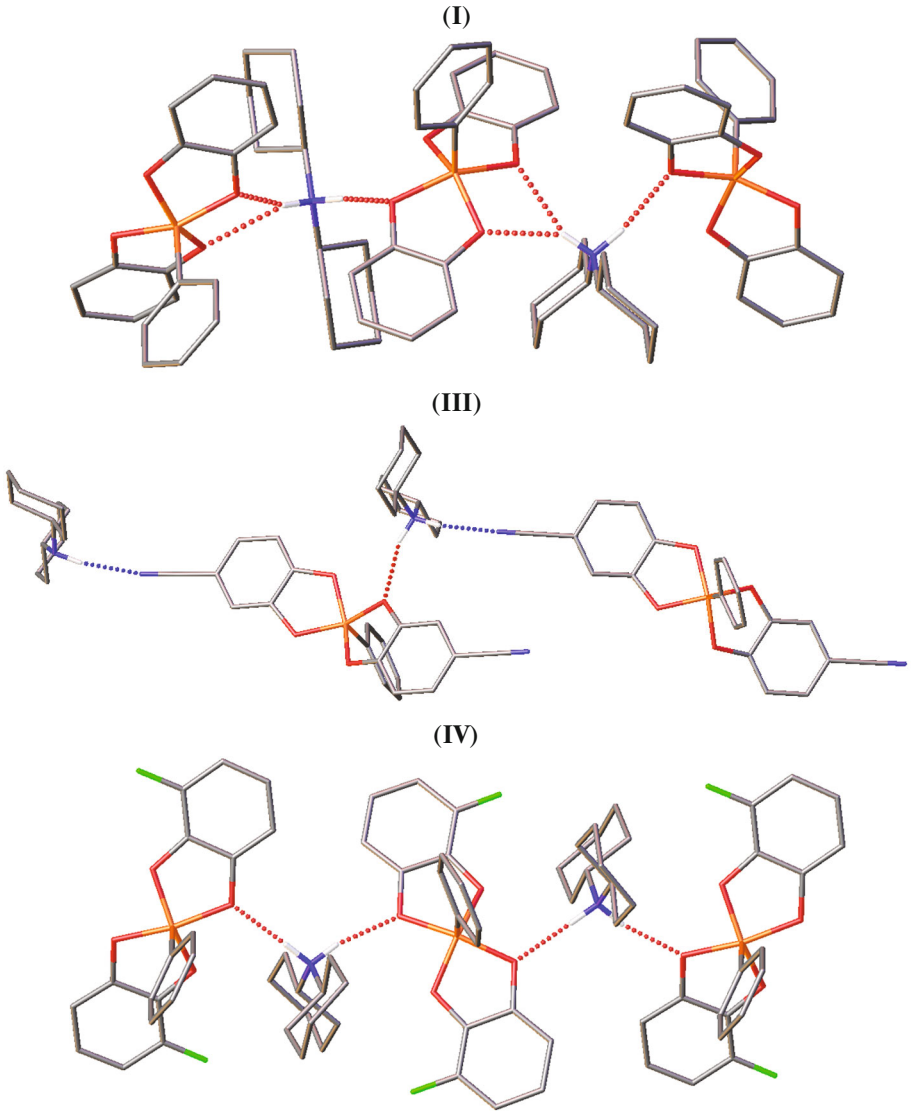

Fig. 6. Hydrogen-bonded chains in structures **I**, **III**, and **V**. The hydrogen atoms not involved in hydrogen bonds are omitted.

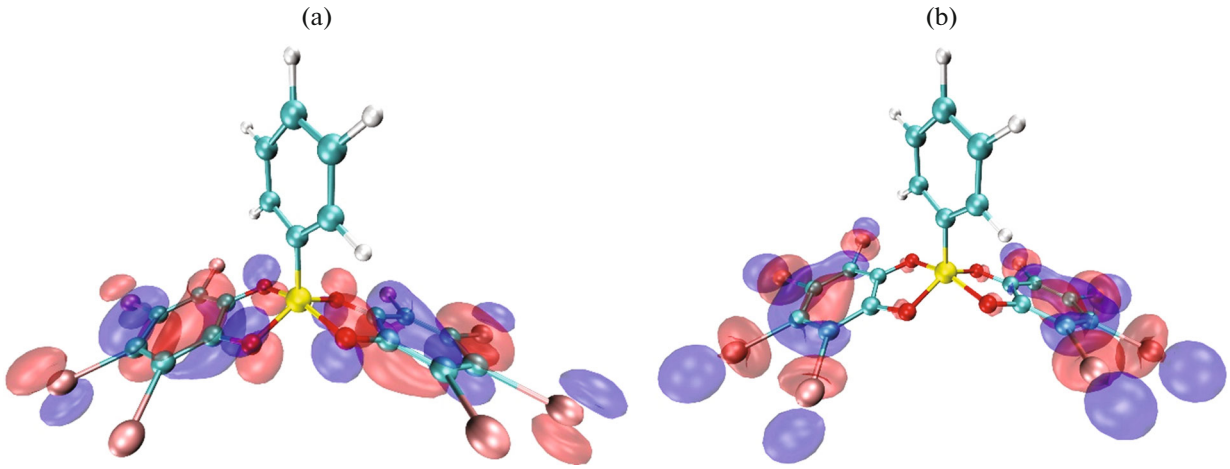

Fig. 7. (a) HOMO and (b) LUMO of the anionic complex **II**. Positive values are shown in blue, negative values are red; the isocontour is 0.03.

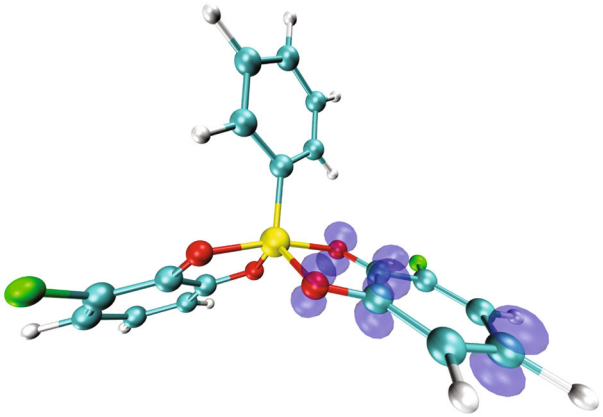

Fig. 8. Spin density distribution in the oxidized form of **V***; the isocontour is 0.03 a.u.

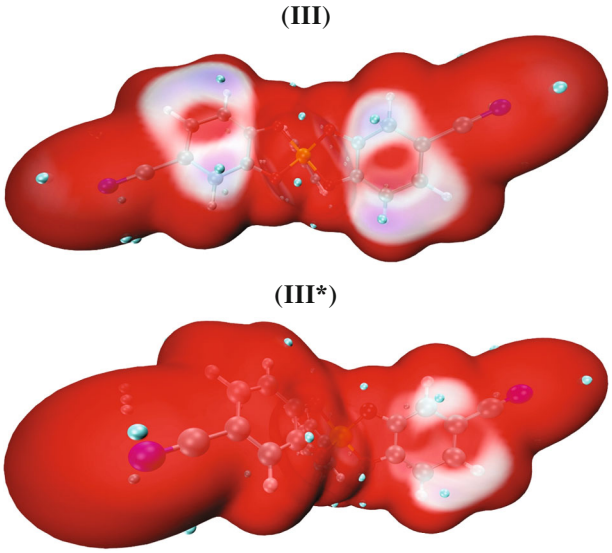

Fig. 9. Distribution of the ALIE function on the electron density isosurface (ρ = 0.005 a.u.) for **III** and **III***. The smallest ALIE values are shown in blue, the largest ones are in red, the minima of ALIE are indicated by green spheres. The range of the values is 0.31 to 0.38 a.u.

inherent in **IV** with the 4-nitrocatecholate ligand. The adiabatic ionization potential obeys a different dependence: the highest value is observed for anionic complex **II** with the tetrabromocatecholate ligand, and the value for **IV** is only slightly lower. The lowest value is typical of complex **I** with unsubstituted catecholate ligand. Apparently, the large number of electron-withdrawing substituents is a stabilization factor of the oxidized forms via the inductive effect. The nitro group in position 4 can also efficiently stabilize the neutral semiquinone catecholate radical complex by not only inductive, but also negative mesomeric effect. The adiabatic potentials can be used to calculate the oxidation potentials According to published data [16], this requires the free energy spent for the oxidation and solvation of anionic complexes and their oxidized forms. Taking account of the free solvation energy results in a pronounced overestimation of the calculated ionization potential relative to the experimental one (Table S7–S9). This is possibly due to specific interactions in solution, which cannot be fully included in quantum chemical calculations. One more possible reason of errors is the value of absolute electrochemical potential of the electrode versus Fc/Fc^+ in DMSO. We used the calculated value (5.04 V [28]), since experimental value could not be found in the literature. Therefore, the calculated oxidation potentials can be taken as relative characteristics reflecting the tendency of anionic complexes **I**–**VI** for oxidation. The highest oxidation potential was found for anionic complexes **II** and **IV**, with the value for the latter being somewhat higher. Although quantum chemical calculations predict the reverse relationship of E^0 for **II** and **IV**, they both still possess the highest oxidation potentials (Table S9).

The oxidation potentials of **II**–**V** were measured in DMSO using voltammetry (Fig. S1). The current–voltage curves for these compounds (except for **II**) show the presence of one oxidation potential at 0.80–0.99 V. The oxidation is irreversible. The highest first oxidation potentials are detected for tetrabromo- and 4-nitrocatecholate ligands (0.90 and 0.99 V). For other compounds, the E^0 values are actually equal (for **III**, **V**, and **VI**, they are 0.83, 0.80, and 0.81 V).

The formation of radical cations and anions in the case of **II** was detected by ESR during the electrochemical oxidation and reduction in acetonitrile, respectively (Fig. S2). Broadened spectra of radical cations and anions were recorded (0.132 and 0.139 mT, respectively); together with moderate intensity and short lifetime, this precludes reliable determination of HFC constants on the silicon atoms; however, the measured *g*-factors of the radical cations and anions are 2.0060 and 2.0050, which corresponds to one unpaired electron. These results indicate that the structure of molecular moieties may be different in the case of oxidation and reduction.

ACKNOWLEDGMENTS

Elemental analysis, X-ray diffraction studies, and recording of NMR and IR spectra were supported by the Ministry of Science and Higher Education of the Russian Federation and performed using research equipment of the Molecular Structure Investigation Center of the Nesmeyanov Institute of Organoelement Compounds, Russian Academy of Sciences. P.A. Buikin and A.A. Korlyukov are grateful to the Interdepartmental Supercomputer Center, Russian Academy of Sciences, for providing access to computational resources and software.

FUNDING

This study was supported by the Russian Foundation for Basic Research (grant no. 19-29-08021).

CONFLICT OF INTEREST

The authors declare that they have no conflicts of interest.

SUPPLEMENTARY INFORMATION

The online version contains supplementary material available at https://doi.org/10.1134/S1070328422090019.

REFERENCES

1. Corce, V., Chamoreau, L.-M., Derat, E., et al., *Angew. Chem., Int. Ed. Engl.*, 2015, vol. 54, no. 39, p. 11414. https://doi.org/10.1002/anie.201504963
2. Raynor, K.D., May, G.D., Bandarage, U.K., et al., *Org. Chem.*, 2018, vol. 83, no. 3, p. 1551. https://doi.org/10/gcts7f
3. Lin, K., Wiles, R.J., Kelly, C.B., et al., *ACS Catal.*, 2017, vol. 7, no. 8, p. 5129. https://doi.org/10/gbrr5s
4. Levernier, E., Corcé, V., Rakotoarison, L.-M., et al., *Org. Chem. Front.*, 2019, vol. 6, no. 9, p. 1378. https://doi.org/10/gpchtm
5. Lévêque, C., Chenneberg, L., Corcé, V., et al., *Org. Chem. Front.*, 2016, vol. 3, no. 4, p. 462. https://doi.org/10/gjz9bm
6. Patel, N.R., Kelly, C.B., Siegenfeld, A.P., et al., *ACS Catal.*, 2017, vol. 7, no. 3, p. 1766. https://doi.org/10/gpcj27
7. Cartier, A., Levernier, E., Corcé, V., et al., *Angew. Chem.*, 2019, vol. 131, no. 6, p. 1803. https://doi.org/10/gpcj3m
8. Levernier, E., Jaouadi, K., Zhang, H.-R., et al., *Chem.-Eur. J.*, 2021, vol. 27, no. 34, p. 8782. https://doi.org/10/gpcj4s
9. Blessing, R.H., *Acta Crystallogr., Sect. A: Found. Crystallogr.*, 1995, vol. A51, no. 1, p. 33. https://doi.org/10.1107/S0108767394005726
10. *APEX3 Suite for Crystallographic Software — Single Crystal X-ray Diffraction*, Bruker AXS, 2014.
11. Dolomanov, O.V., Bourhis, L.J., Gildea, R.J., et al., *J. Appl. Crystallogr.*, 2009, vol. 42, no. 2, p. 339. https://doi.org/10.1107/S0021889808042726
12. Sheldrick, G.M., *Acta Crystallogr., Sect. A: Cryst. Adv.*, 2015, vol. 71, no. 1, p. 3. https://doi.org/10.1107/S2053273314026370
13. Sheldrick, G.M., *Acta Crystallogr., Sect. C: Struct. Chem.*, 2015, vol. 71, no. 1, p. 3. https://doi.org/10.1107/S2053229614024218
14. Krylov, A.I. and Gill, P.M.W., *WIREs Comput. Mol. Sci.*, 2013, vol. 3, no. 3, p. 317. https://doi.org/10/f4wfdf
15. Epifanovsky, E., Gilbert, A.T.B., Feng, X., et al., *J. Chem. Phys.*, 2021, vol. 155, no. 8, p. 084801. https://doi.org/10/gmxp67
16. Neugebauer, H., Bohle, F., Bursch, M., et al., *J. Phys. Chem. A*, 2020, vol. 124, no. 35, p. 7166. https://doi.org/10/gnv5m6
17. Lu, T. and Chen, F., *J. Comput. Chem.*, 2012, vol. 33, no. 5, p. 580. https://doi.org/10.1002/jcc.22885
18. Humphrey, W., Dalke, A., and Schulten, K., *J. Mol. Graph.*, 1996, vol. 14, no. 1, p. 33. https://doi.org/10/b3tgfk
19. Boer, F.P., Flynn, J.J., and Turley, J.W., *J. Am. Chem. Soc.*, 1968, vol. 90, no. 25, p. 6973. https://doi.org/10/dx7qfc
20. Holmes, R.R., Day, R.O., Chandrasekhar, V., et al., *Inorg. Chem.*, 1985, vol. 24, no. 13, p. 2009. https://doi.org/10/dpfxj2
21. Holmes, R.R., Day, R.O., Harland, J.J., et al., *Organometallics*, 1984, vol. 3, no. 3, p. 341. https://doi.org/10/b9kkvp
22. Holmes, R.R. and Deiters, J.A., *J. Am. Chem. Soc.*, 1977, vol. 99, no. 10, p. 3318. https://doi.org/10.1021/ja00452a021
23. Korlyukov, A.A., *Usp. Khim.*, 2015, vol. 84, no. 4, p. 422.
24. Kramarova, E.P., Volodin, A.D., Negrebetsky, V.V., et al., *Molecules*, 2021, vol. 26, no. 12, p. 3548. https://doi.org/10.3390/molecules26123548
25. Korlyukov, A.A., Shipov, A.G., Kramarova, E.P., et al., *Izv. Akad. Nauk. Ser. Khim.*, 2008, no. 10, p. 2055.
26. O'Keeffe, M., Peskov, M.A., Ramsden, S.J., et al., *Acc. Chem. Res.*, 2008, vol. 41, no. 12, p. 1782. https://doi.org/10/fwg963
27. Politzer, P. and Murray, J.S., *Theoretical and Computational Chemistry, Chapter 8: The Averag Local Ionization Energy: Concepts and Applications*, Toro-Labbe, A., Ed., 2007, vol. 19, p. 119. https://doi.org/10.1016/S1380-7323(07)80009-4
28. Namazian, M., Lin, C.Y., and Coote, M.L., *J. Chem. Theory Comput.*, 2010, vol. 6, no. 9, p. 2721. https://doi.org/10/bqb274

Translated by Z. Svitanko